Magnetic coupling in the insulating and metallic ferromagnetic $La_{1-x}Ca_xMnO_3$

Pengcheng Dai,[1,2] J. A. Fernandez-Baca,[2] E. W. Plummer,[1,2] Y. Tomioka,[3,4] and Y. Tokura[3,4,5]
[1]*Department of Physics and Astronomy, The University of Tennessee, Knoxville, Tennessee 37996*
[2]*Solid State Division, Oak Ridge National Laboratory, Oak Ridge, Tennessee 37831-6393*
[3]*Joint Research Center for Atom Technology (JRCAT), Tsukuba 305-0046, Japan*
[4]*Correlated Electron Research Center (CERC), AIST, Tsukuba 305-8562, Japan*
[5]*Department of Applied Physics, University of Tokyo, Tokyo 113-8656, Japan*
(Received 31 January 2001; revised manuscript received 16 August 2001; published 26 November 2001)

Low-energy spin excitations play an essential role in determining the characteristics of the phase transitions in the colossal magnetoresistant manganese-oxides (manganites). Inelastic neutron scattering has been utilized to study the spin excitations of the ferromagnetic (FM) $La_{1-x}Ca_xMnO_3$ (LCMO) as a function of hole doping x (0.2, 0.25, and 0.30) and temperature, above and below the Curie temperature T_C. While the spin-diffusion coefficients $\Lambda(T)$ and T_C's increase smoothly with doping concentration x, the spin-stiffness constant $D(T)$ for the insulating LCMO is 3 times smaller than that of the metallic LCMO. Furthermore, the paramagnetic-to-ferromagnetic phase transitions in LCMO manganites investigated have nonvanishing extrapolated values of $D(T)$ as $T \rightarrow T_C$ and nondiverging spin-correlation lengths at T_C. These results present a serious challenge to the understanding of these materials using models such as Heisenberg ferromagnetism, double exchange, or modified double exchange.

DOI: 10.1103/PhysRevB.64.224429 PACS number(s): 72.15.Gd, 61.12.Ld, 71.30.+h

The elementary spin excitations in a ferromagnet can provide direct information about the magnetic interactions from the spins associated with the unpaired electrons in the system. Below the Curie temperature T_C, when the spins order ferromagnetically, the elementary magnetic excitations are propagating spin waves. The energy change of the system for a small magnetic disturbance with wave vector q is characterized by the spin-wave stiffness coefficient $D(T)$ for small q.[1] Above T_C in the spin-disordered paramagnetic (PM) state, the spin excitations can only propagate through the spin-diffusion process and the response of the system for the same magnetic disturbance is measured by the spin-diffusion coefficient $\Lambda(T)$.[2] In the hydrodynamic limit of long wavelengths (small q) and small frequencies, $D(T)$ and $\Lambda(T)$ are related to the spin-wave energy $\hbar\omega$ and the energy width of the magnetic diffuse scattering $\Gamma(q)$ via the quadratic form $\hbar\omega = \Delta + Dq^2$ and $\Gamma(q) = 1/\tau = \Lambda q^2$, where Δ is the small dipolar gap arising from the spin anisotropy and τ is the spin-relaxation time.

In the mixed-valent ferromagnetic (FM) manganese oxides $A_{1-x}B_xMnO_3$ (A is trivalent and B divalent ion), the ferromagnetic-to-paramagnetic transition is intimately related to a metal-to-insulator (MI) transition.[3] The basic microscopic mechanism for such behavior is believed to be the double-exchange (DE) interaction,[4] where FM coupling between localized Mn t_{2g} spins is mediated by the hopping of e_g electrons [with kinetic energy (KE)] which enables the avoidance of the Hund's-rule energy (J_H). The DE model makes clear predictions about the nature of the spin excitations and their dependence upon the electronic bandwidth, KE, T_C, and doping concentration x. In the semiclassical approximation of this model, the spin-wave dispersion of the ferromagnet can be mapped onto that of a nearest-neighbor Heisenberg Hamiltonian.[5–8] For FM $A_{1-x}B_xMnO_3$ with $x \approx 0.3$, the T_C's and zero-temperature electric conductivity can be continually suppressed by different $A(B)$ substitutions until an insulating, charge-ordered ground state is stabilized.[9] When the average ionic size of ions $A(B)$ is small, the system is insulating. As the ionic size $A(B)$ becomes larger, the system turns into a metal. Although such ionic size effect is commonly thought to originate from its dependence of the electronic bandwidth through the bending of the Mn-O-Mn bond,[9] systematic neutron scattering measurements show that a number of features in spin-wave excitations of $A_{0.7}B_{0.3}MnO_3$ are inconsistent with such a description. In particular, spin-wave excitations of the low-T_C $A_{0.7}B_{0.3}MnO_3$ cannot be described from the nearest-neighbor Heisenberg Hamiltonian.[10–12] First, there is an anomalous central diffusive component in spin-wave excitations for $A_{0.7}B_{0.3}MnO_3$ as T_C is approached.[10] Second, the FM spin-wave stiffness $D(T)$ for $A_{0.7}B_{0.3}MnO_3$ that should follow the electronic bandwidth and T_C exhibits little composition dependence.[11] Finally, anomalous zone-boundary spin-wave softening and broadening are observed for the low-T_C $A_{0.7}B_{0.3}MnO_3$ manganites.[12]

Although some features of spin-wave excitations in $A_{0.7}B_{0.3}MnO_3$ deviate from expectations of the semiclassical approximation of the DE model, considerations of the exact solution of the DE model for finite systems,[13–15] approximate calculations of DE for infinite systems,[16] or orbital effects in addition to the DE mechanism[17,18] may explain the anomalous results.[10–12] For example, large zone-boundary magnon softening and broadening are natural consequences of the more precise calculations of the DE model[13–16] or orbital effects in addition to the DE-mechanism.[17,18] Since these theories in their present forms[13–18] are not expected to affect the small-momentum spin excitations, it is interesting to explore these excitations in a range of doping x below and above T_C. If a current DE-based model is sufficient to explain the properties of $A_{0.7}B_{0.3}MnO_3$,[13–18] it should also account for the doping dependence of the spin excitations.

For a conventional cubic Heisenberg ferromagnet with only nearest-neighbor spin exchange interaction, $D(0)$ scales with the magnitude of the exchange coupling J.[1] Since the latter also controls the T_C, the ratio of $D(0)/kT_C$ is expected to be a constant.[1] Previous work on FM metallic $A_{0.7}B_{0.3}MnO_3$ found that $D(0)/kT_C$ values deviate from such behavior and become larger for materials with lower T_C's.[11] However, because the low-T_C materials also have nonvanishing $D(T)$ at T_C, the T_C's in these materials are thought to be prematurely terminated by the appearance of lattice and magnetic polarons.[19,20] In the strong-coupling limit (KE$\ll J_H$) of a DE ferromagnet, $D(0)$ (Refs. 5–8) and Λ (Ref. 21) are found to be approximately proportional to KE, T_C, and x for small x. Even in the exact calculations,[13–15] $D(0)$ is expected to closely follow the Heisenberg Hamiltonian and increase smoothly with x for $0.15 \leqslant x \leqslant 0.45$. For the FM $La_{1-x}Sr_xMnO_3$ (LSMO), neutron scattering measurements indeed show that the expected behavior for $D(0)$ as a function of x is observed.[22–24]

In this article, we use neutron scattering to demonstrate that the doping dependence of the spin excitations in FM $La_{1-x}Ca_xMnO_3$ (LCMO) is unexpected from the Heisenberg or current DE-based models.[5–8,13–18] Although the T_C's of the LCMO increase smoothly with increasing hole doping for $0.2 \leqslant x \leqslant 0.33$,[25] we show that $D(0)$ and Λ, measured at low T and $1.1T_C$, respectively, have dramatically different doping dependence as one goes from the insulating $La_{0.8}Ca_{0.2}MnO_3$ (LCMO20, $T_C = 178 \pm 1$ K as determined by the *in situ* elastic neutron diffraction on the [1,0,0] and [1,1,0] Bragg peaks) to the metallic $La_{0.75}Ca_{0.25}MnO_3$ (LCMO25, $T_C = 191 \pm 1$ K) and $La_{0.7}Ca_{0.3}MnO_3$ (LCMO30, $T_C = 238 \pm 1$ K).[19] In contrast to the expected linear doping-dependent behavior for $D(0)$ and Λ [i.e., $D(0) \propto \Lambda \propto x$], $D(0)$ of LCMO20 was found to be 3 times smaller than that of LCMO25 and LCMO30 while Λ at $1.1T_C$ is proportional to x. In addition, the ferromagnetic-to-paramagnetic transitions in all three ferromagnets have nonvanishing extrapolated values of $D(T)$ as $T \rightarrow T_C$ and nondiverging spin-correlation lengths at T_C. The spin excitations of the metallic LCMO25 and LCMO30 are dominated by the spin-diffusive process as $T \rightarrow T_C$,[10,11] while no evidence of the same behavior was found in the insulating LCMO20 below T_C. Since $D(T)$ and Λ measure the spin response of a ferromagnet to an external magnetic disturbance below and above T_C, the surprising result of their different doping dependence in LCMO presents a challenge to the understanding of these materials using models such as Heisenberg ferromagnetism, double exchange, or modified double exchange.

Our experiments were carried out on the HB-1 and HB-1A triple-axis spectrometers at the High-Flux Isotope Reactor of Oak Ridge National Laboratory.[11,12] We have used pyrolytic graphite (PG) as the monochromator and crystals of PG or Be as the analyzer with the final neutron energy fixed at $E_f = 13.6$ meV (2.46 Å). Most of the measurements were performed using Be(1,0,1) as analyzer with collimations of, proceeding from the reactor to the detector, 40-20-40-120 min [full width at half maximum (FWHM)]. Such a spectrometer setup provides an energy resolution at the elastic ($\hbar\omega = 0$) position of $\Delta E = 0.5$ meV. The twinned LCMO single crystals have O'-orthorhombic structure slightly distorted from the cubic lattice.[26–28] For simplicity we use a pseudocubic unit cell with lattice parameters of $a \approx b \approx c \approx 3.87$ Å, 3.87 Å, and 3.86 Å for LCMO20, LCMO25, and LCMO30, respectively. The momentum transfers $Q = (q_x, q_y, q_z)$ in units of Å^{-1} are at positions $(H,K,L) = (q_x a/2\pi, q_y a/2\pi, q_z a/2\pi)$ in reciprocal lattice units (rlu). The crystals were oriented to allow wave vectors of the form (H,K,K) to be accessible in the horizontal scattering plane.

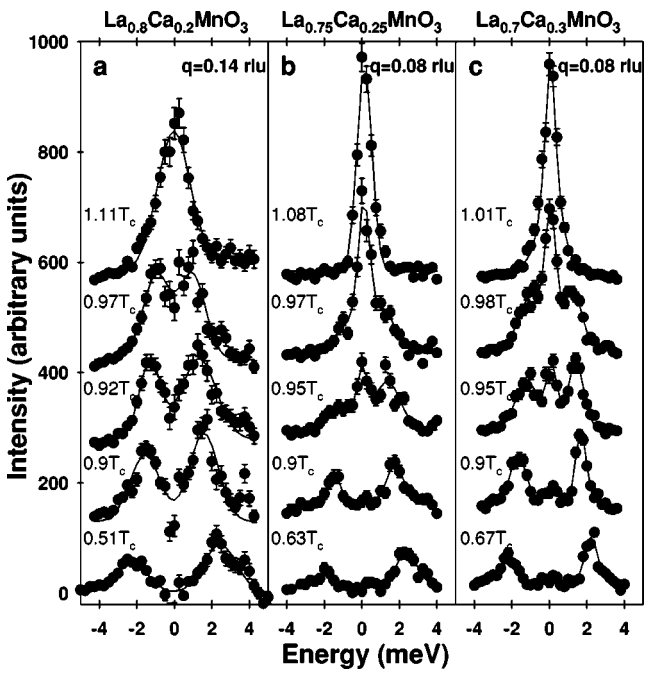

FIG. 1. Constant-q scans at $[1+q,0,0]$ for LCMO20 at $q = 0.14$ rlu (a), LCMO25 at $q = 0.08$ rlu (b), and LCMO30 at $q = 0.08$ rlu (c). The solid lines are resolution-limited Gaussian fits to the data. The weak nonmagnetic contribution to the scattering at $\hbar\omega = 0$ has been subtracted from identical measurements at 10 K (see Refs. 10 and 11.)

Figure 1 shows representative constant-q inelastic neutron scans at various temperatures for LCMO20, LCMO25, and LCMO30. Below $0.9T_C$, well-defined spin-wave peaks are found in the neutron energy gain ($\hbar\omega < 0$) and energy loss ($\hbar\omega > 0$) sides for all three samples. At low temperatures, all three data sets show spin-wave excitations of similar energies. However, the wave vectors are at $q = 0.08$ rlu for LCMO25 and LCMO30 [Figs. 1(b) and 1(c)] and at $q = 0.14$ rlu for LCMO20 [Fig. 1(a)]. Since the spin-wave energy follows the quadratic dependence on q, this means that $D(0)$ for LCMO20 is considerably smaller than that for LCMO25 and LCMO30. For insulating LCMO20 [Fig. 1(a)], the excitations soften and become more intense as $T \rightarrow T_C$. For LCMO25 and LCMO30, which exhibit MI transitions around T_C,[25] the excitations show a slow spin-wave energy renormalization and domination of a central diffusive component in the spectra for $T > 0.9T_C$. As shown in Figs. 1(b) and 1(c), the growth of the central component in LCMO20 and LCMO25 as $T \rightarrow T_C$ is at the expense of spin-wave

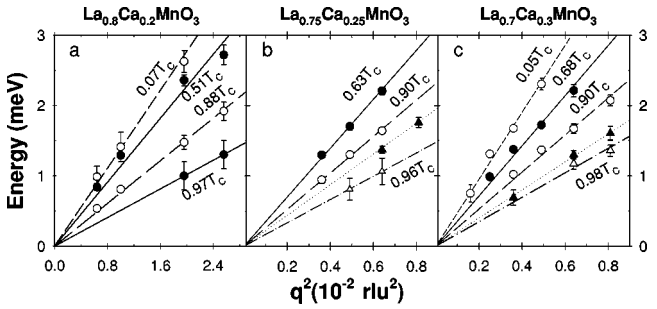

FIG. 2. Spin-wave energy vs wave vector used to determine the spin-wave stiffness $D(T)$ at various temperatures for (a) LCMO20, (b) LCMO25, and (c) LCMO30. Note the differences in the wave vector values between LCMO20 and LCMO25.

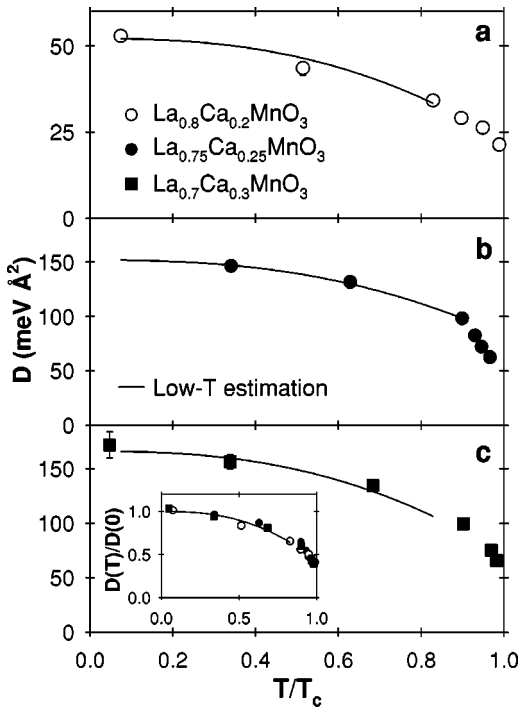

FIG. 3. Spin-wave stiffness $D(T)$ vs T/T_C for LCMO20 (open circles), LCMO25 (solid circles), and LCMO30 (solid squares). The solid line is the estimated T dependence of the $D(T)$ using $D(T)=D(0)(1-AT^{5/2})$. The inset in (c) shows the normalized spin-wave stiffness $D(T)/D(0)$ vs T/T_C for LCMO20, LCMO25, and LCMO30.

excitations.[10,11,20] Its absence in the insulating LCMO20 at $T<T_C$ suggests that the appearance of the central diffusive component in LCMO25 and LCMO30 below T_C is intimately related to the MI transitions in these materials.

For a Heisenberg ferromagnet, the T dependence of the spin-wave stiffness is expected to follow mode-mode coupling theory with $D(T)=D(0)(1-AT^{5/2})$ at low T/T_C. As $T\rightarrow T_C$, $D(T)$ should renormalize to zero at T_C as $[(T-T_C)/T_C]^{\nu-\beta}$ with $\nu-\beta=0.34$.[29] To determine if $D(T)$ in LCMO follows the expected behavior, we measured the spin-wave dispersion curves at small wave vectors. Figure 2 shows the outcome of $D(T)$ obtained by fitting the dispersion using $\hbar\omega=\Delta+Dq^2$. In all three cases, a very small dipolar ($\Delta\leqslant 0.05$ meV) energy gap was found and for practical purposes neglected. In Fig. 3, $D(T)$ derived from the dispersion curves in Fig. 2 is plotted as a function of T/T_C for LCMO20, LCMO25, and LCMO30. Three important conclusions can be drawn from the figure. First, $D(0)$ for the insulating LCMO20 is roughly 3 times smaller than that for the metallic LCMO25 and LCMO30. Second, $D(T)$ shows no evidence for the expected spin-wave collapse at T_C. Finally, the normalized spin stiffness $D(T)/D(0)$ for all three ferromagnets exhibits almost the same T dependence as $T\rightarrow T_C$ [see the inset of Fig. 3(c)] even though the spin excitations of LCMO20 do not have the central diffusive component below T_C. Therefore, the $D(0)/kT_C$ value for LCMO exhibits opposite behavior from that of $A_{0.7}B_{0.3}MnO_3$ and becomes smaller for the lower-T_C LCMO20. This is difficult to understand within the Heisenberg Hamiltonian.

Although measurements of $D(T)$ can determine an effective J in the FM state, information concerning the magnetic interaction and relaxation in the PM state can only be obtained through measuring the spin-diffusion coefficient $\Lambda(T)$. To establish the doping dependence of $\Lambda(T)$, we measured the intrinsic energy width $\Gamma(q)$ of the central diffusive component as a function of wave vector q at $1.1T_C$ for LCMO20, LCMO25, and LCMO30. The magnetic central diffusive scattering was obtained by subtracting the low-T weak nonmagnetic elastic incoherent scattering at $\hbar\omega=0$ meV from the measurements at $1.1T_C$. The left and right panels of Fig. 4 show the wave vector dependence of the central diffuse scattering for LCMO20 and LCMO25, respectively. In contrast to the wave vector dependence of the spin wave energy below T_C (Fig. 1), the wave vector dependence of the energy width for the spin central diffusive component is almost identical for insulating LCMO20 and metallic LCMO25 at $1.1T_C$ (left and right panels of Fig. 4). We fitted the measured $\Gamma(q)$ to $\Gamma(q)=\Lambda q^2$ and the outcome of the fit is shown in Fig. 5(a). For completeness, we also included the Λ for LCMO33.[10] Clearly, Λ increases smoothly with increasing x for LCMO and shows no dramatic difference in its value for insulating or metallic LCMO. In the $KE\ll T\ll J_H$ limit, the DE model gives $\Lambda\propto KE\propto tx(1-x)$, where t is the usual electron hopping amplitude.[21] This means that, to the lowest order, Λ should be proportional to x, a prediction that is consistent with the results of Fig. 5(a).

However, in the same $KE\ll J_H$ limit, the DE model predicts that the low-T spin stiffness $D(0)$ should also be proportional to x.[5–8] In Fig. 5(b), we plot the doping dependence of the spin-wave stiffness measured on the same samples at 10 K. On increasing the doping from $x=0.2$ to 0.25, $D(0)$ shows a threefold jump in magnitude (from 50 meV Å^2 for LCMO20 to 150 meV Å^2 for LCMO25) while the T_C and Λ values for these two materials are essentially the same. On further increasing the doping from LCMO25 to LCMO30, both $D(0)$ and $\Lambda(1.1T_C)$ increase slightly (Fig. 5). Thus, while $D(0)$ and $\Lambda(1.1T_C)$ are probing the magnetic response of a ferromagnet below and above T_C, the differences in their doping dependence for LCMO suggest that these values are controlled by different magnetic interac-

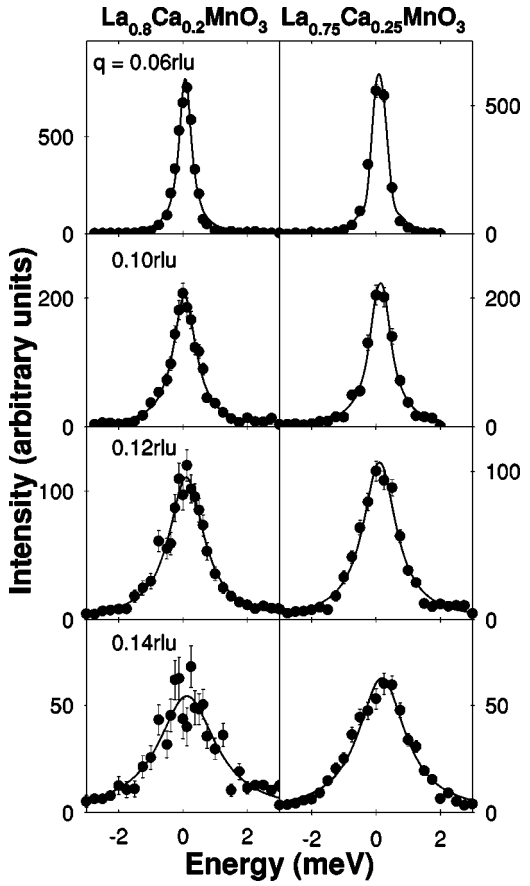

FIG. 4. Energy dependence of the paramagnetic scattering at various wave vectors at $T \approx 1.1T_C$ for LCMO20 (left panel) and LCMO30 (right panel). The data are used to determine the spin-diffusion coefficients Λ using $\Gamma(q) = \Lambda q^2$ for LCMO20 and LCMO25. Note that the energy widths for LCMO20 and LCMO25 are similar at the same wave vectors.

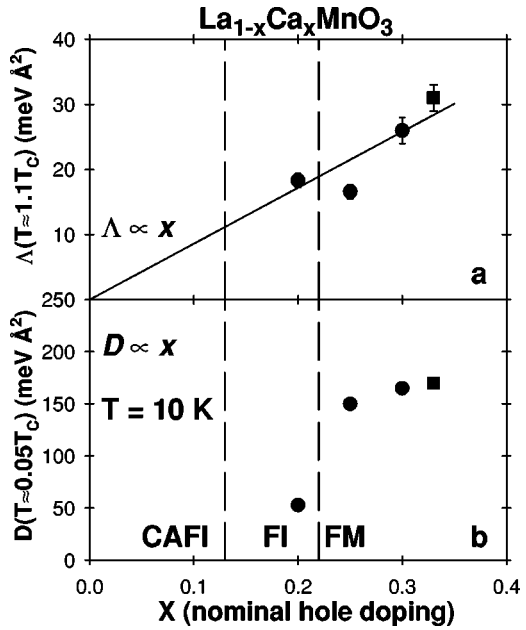

FIG. 5. Λ at $T \approx 1.1T_C$ (a) and D at 10 K (b) as a function of nominal hole doping x for LCMO. The estimated phase boundaries for canted AF insulator (CAFI), FM insulator (FI), and FM metal (FM) are marked by dashed lines. The error bars are given by vertical lines or smaller than the symbol size. Data for LCMO33 are from Ref. 10.

tions. As the unmodified DE model predicts a FM metallic phase when $0 < x < 1$, the observation of an insulating FM LCMO20 suggests that ferromagnetism in this material originates from superexchange interaction.[30] Alternatively, if DE still applies to LCMO20, its insulating behavior may be the consequence of polaron and orbital ordering.[31]

To further establish the nature of the FM phase transitions in LCMO20 and LCMO25, we performed systematic static wave-vector-dependent susceptibility $\chi_{\mathbf{q}}(\hbar\omega = 0)$ and static spin-spin correlation length measurements.[11,29] For a conventional second-order FM phase transition, the spin susceptibility should show a cusp at the FM transition and the spin-spin correlation length is expected to diverge at T_C.[29] The T dependence of $\chi_{\mathbf{q}}(\hbar\omega = 0)$ for LCMO20 and LCMO25 at several wave vectors is shown in Figs. 6(a) and 6(b). While the data for LCMO20 have a well-defined cusp at T_C [Fig. 6(a)], $\chi_{\mathbf{q}}(\hbar\omega = 0)$ at identical wave vectors for LCMO25 shows broadened peaks with maxima at temperatures somewhat below T_C similar to other low-T_C $A_{0.7}B_{0.3}MnO_3$ manganites.[11] To obtain the spin-spin correlation lengths, we least-square-fitted the measured static spin correlation at each T to an Ornstein-Zernike cross section [i.e., $I \propto 1/(\kappa^2 + q^2)$] convoluted with the instrumental resolution.[29] From the fits at various temperatures we extracted the spin-correlation length $\xi(T)$ via $\xi(T) = 1/\kappa(T)$, where $\kappa(T)$ measures the width of the spin-correlation function in $Å^{-1}$. Figures 6(c) and 6(d) show the T dependence of ξ for LCMO20 and LCMO25,

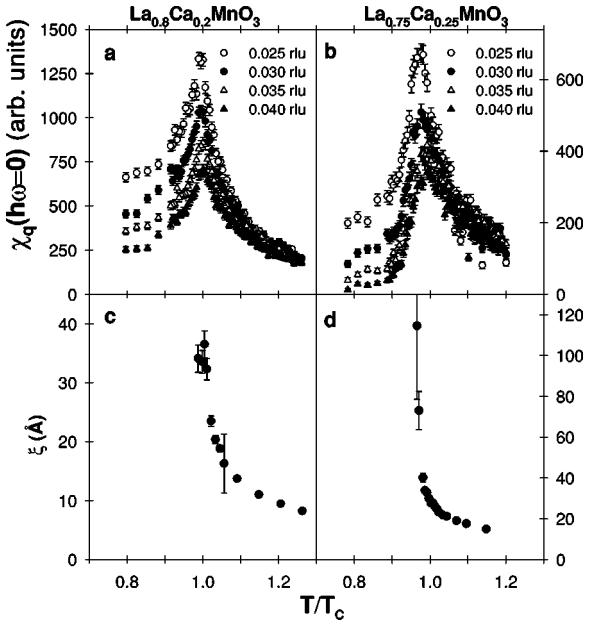

FIG. 6. (a) Temperature dependence of the static wave-vector-dependent susceptibility $\chi_{\mathbf{q}}(\hbar\omega = 0)$ for LCMO20. (b) $\chi_{\mathbf{q}}(\hbar\omega = 0)$ for LCMO25. The energy resolution of the spectrometer at elastic position is about 0.4 meV. The T dependence of the spin-correlation length $\xi(T)$ for (c) LCMO20 and (d) LCMO25.

respectively. For LCMO20, $\xi(T)$ increases from ~ 10 Å to 35 Å as $T \rightarrow T_C$ but does not diverge at T_C. Similarly, $\xi(T)$ for LCMO25 remains small (≈ 30 Å) at T_C and grows to over 100 Å only at temperatures below T_C. Therefore, FM LCMO manganites have nonvanishing spin stiffness $D(T)$ and nondiverging spin-correlation length $\xi(T)$ at T_C, suggesting unconventional FM phase transitions in these materials.[32]

Clearly, the spin dynamics of LCMO exhibits a variety of intriguing properties that are unexpected from Heisenberg[1] or the current DE-based models.[5–8,13–18,21] In particular, the large difference in $D(0)$ for LCMO20 and LCMO25 that have similar T_C's and spin-diffusion coefficients is puzzling. If the strange magnetism and the resistivity rise in LCMO20 (Refs. 25 and 19) are due to the segregation of the material into metallic and insulating phases,[33] one would expect that the metallic regions are FM and the insulating regions are either antiferromagnetic (AF) with the AF component below our detection limit or PM. In this scenario, the $D(0)$ stemming from the FM metallic regions of the sample should increase smoothly with x and be independent of the bulk resistivity. Clearly, this is not observed in Fig. 5(b). Since the neutron is a bulk probe with a coherence length of ~ 300 Å, our results indicate that the low-T insulating behavior in LCMO20 cannot be due to the micron-sized metallic FM clusters inside the insulating AF/PM matrix as suggested from the tunneling experiments.[34] However, whether the anomalous spin excitations in LCMO can be induced by the nanometer-sized short-range charge correlations in LCMO (Ref. 19) or not is unclear.

In summary, neutron scattering was used to investigate the spin excitations in FM LCMO for the doping range $0.2 \leqslant x \leqslant 0.3$. We establish the doping dependence of the spin-wave stiffness and the spin-diffusion coefficients. We find that $D(0)/kT_C$ for LCMO does not follow the expectations of Heisenberg ferromagnets. Although $D(0)$ and Λ are probing the energy changes of the system for a small magnetic disturbance below and above T_C, these two quantities are found to behave differently with doping. While Λ around T_C for LCMO increases smoothly with increasing doping, D at low T exhibits a dramatic increase from the insulating LCMO20 to metallic LCMO25. Furthermore, the ferromagnetic-to-paramagnetic phase transitions in LCMO in the hole doping range $0.2 \leqslant x \leqslant 0.3$ have nonvanishing spin-wave stiffness and nondiverging spin-correlation length at T_C.

Note added. After the submission of the present manuscript, we became aware of a related paper by Biotteau and co-workers.[35] These authors reached the same conclusion as the present paper about the weak spin-wave stiffness for $La_{1-x}Ca_xMnO_3$ with $x \leqslant 0.2$.

We thank E. Dagotto, R. S. Fishman, T. A. Kaplan, G. Khaliullin, and Jiandi Zhang for helpful discussions. This work was supported by the U.S. DOE under Contract No. DE-AC05-00OR22725 with UT-Battelle, LLC, by JRCAT of Japan, and by NSF Grant No. DMR-0072998.

[1] S. W. Lovesey, *Theory of Thermal Neutron Scattering from Condensed Matter* (Clarendon, Oxford, 1984), Vol. 2, Chap. 9.
[2] B. Halperin and P. C. Hohenberg, Phys. Rev. **188**, 898 (1969).
[3] G. H. Jonker and J. H. Van Santen, Physica (Amsterdam) **16**, 337 (1950).
[4] C. Zener, Phys. Rev. **82**, 403 (1951).
[5] K. Kubo and N. Ohata, J. Phys. Soc. Jpn. **33**, 21 (1972).
[6] N. Furukawa, J. Phys. Soc. Jpn. **65**, 1174 (1996).
[7] X. D. Wang, Phys. Rev. B **57**, 7427 (1998).
[8] M. Quijada, J. Cerne, J. R. Simpson, H. D. Drew, K. H. Ahn, A. J. Millis, R. Shreekala, R. Ramesh, M. Rajeswari, and T. Venkatesan, Phys. Rev. B **58**, 16 093 (1998).
[9] H. Y. Hwang, S.-W. Cheong, P. G. Radaelli, M. Marezio, and B. Batlogg, Phys. Rev. Lett. **75**, 914 (1995).
[10] J. W. Lynn, R. W. Erwin, J. A. Borchers, Q. Huang, A. Santoro, J. L. Peng, and Z. Y. Li, Phys. Rev. Lett. **76**, 4046 (1996).
[11] J. A. Fernandez-Baca, P. Dai, H. Y. Hwang, C. Kloc, and S.-W. Cheong, Phys. Rev. Lett. **80**, 4012 (1998).
[12] P. Dai, H. Y. Hwang, J. Zhang, J. A. Fernandez-Baca, S.-W. Cheong, C. Kloc, Y. Tomioka, and Y. Tokura, Phys. Rev. B **61**, 9553 (2000); H. Y. Hwang, P. Dai, S.-W. Cheong, G. Aeppli, D. A. Tennant, and H. A. Mook, Phys. Rev. Lett. **80**, 1316 (1998).
[13] J. Zang, H. Roder, A. R. Bishop, and S. Trugman, J. Phys.: Condens. Matter **9**, L157 (1997).
[14] T. A. Kaplan and S. D. Mahanti, J. Phys.: Condens. Matter **9**, L291 (1997); in *Physics of Manganites*, edited by T. A. Kaplan and S. D. Mahanti (Kluwer Academic and Plenum, New York, 1998), p. 135.
[15] T. A. Kaplan, S. D. Mahanti, and Y.-S. Su, Phys. Rev. Lett. **86**, 3634 (2001).
[16] D. I. Golosov, Phys. Rev. Lett. **84**, 3974 (2000).
[17] R. Maezono and N. Nagaosa, Phys. Rev. B **61**, 1189 (2000).
[18] G. Khaliullin and R. Kilian, Phys. Rev. B **61**, 3494 (2000); R. Kilian and G. Khaliullin, *ibid.* **60**, 13 458 (1999).
[19] P. Dai, J. A. Fernandez-Baca, N. Wakabayashi, E. W. Plummer, Y. Tomioka, and Y. Tokura, Phys. Rev. Lett. **85**, 2553 (2000).
[20] C. P. Adams, J. W. Lynn, Y. M. Mukuvskii, A. A. Arsenov, and D. A. Shulyatev, Phys. Rev. Lett. **85**, 3954 (2000).
[21] R. S. Fishman, Phys. Rev. B **62**, R3600 (2000); J. Phys.: Condens. Matter **12**, L575 (2000). These papers find $\Lambda \propto \mathrm{KE} \propto x$ in the high-T limit ($T \gg \mathrm{KE}$). However, the same relation also holds at intermediate T. This is because one electron must occupy each site at half-filling ($x=0$) to avoid the enormous cost in Hund's coupling (J_H). As a consequence, KE and Λ must vanish at $x=0$ for any T and Λ is proportional to x near $x=0$ [R. S. Fishman (unpublished)].
[22] K. Hirota, N. Kaneko, A. Nishizawa, Y. Endoh, M. C. Martin, and G. Shirane, Physica B **237-238**, 36 (1997).
[23] A. H. Moudden, L. Vasiliu-Doloc, L. Pinsard, and A. Revcolevschi, Physica B **241-243**, 276 (1998).

[24] L. Vasiliu-Doloc, J. W. Lynn, Y. M. Mukovskii, A. A. Arsenov, and D. A. Shulyatev, J. Appl. Phys. **83**, 7342 (1998).
[25] T. Okuda, Y. Tomioka, A. Asamitsu, and Y. Tokura, Phys. Rev. B **61**, 8009 (2000).
[26] J. B. Goodenough, A. Wold, R. J. Arnott, and N. Menyuk, Phys. Rev. **124**, 373 (1961).
[27] P. Dai, J. Zhang, H. A. Mook, S.-H. Liou, P. A. Dowben, and E. W. Plummer, Phys. Rev. B **54**, R3694 (1996).
[28] Q. Huang, A. Santoro, J. W. Lynn, R. W. Erwin, J. A. Borchers, J. L. Peng, K. Ghosh, and R. L. Greene, Phys. Rev. B **58**, 2684 (1998).
[29] M. Collins, *Magnetic Critical Scattering* (Clarendon, Oxford, 1989), p. 29.
[30] In Ref. 26, Goodenough *et al.* showed that the superexchange interaction in Mn^{3+}-O^{2-}-Mn^{3+} should be anisotropic, being FM in the *a*-*b* planes and AF along the *c* axis (*A*-type AF), for *O′*-orthorhombic samples ($c/\sqrt{2}<a<b$) with static Jahn-Teller's (JT) distortion. Although LCMO20 has the *O′*-orthorhombic structure (Ref. 28) and short-range static JT distortion below T_C (Ref. 19), magnetic exchange in LCMO20 is isotropic and purely FM. Therefore, Kanamori-Goodenough rule (Ref. 26) may not apply.
[31] In principle, long-range polaron [Y. Yamada, O. Hino, S. Nohdo, R. Kanao, T. Inami, and S. Katano, Phys. Rev. Lett. **77**, 904 (1996)] and/or orbital [Y. Endoh, K. Hirota, S. Ishihara, S. Okamoto, Y. Murakami, A. Nishizawa, T. Fukuda, H. Kimura, H. Nojiri, K. Kaneko, and S. Maekawa, *ibid.* **82**, 4328 (1999)] ordering can give rise to FM insulating behavior. Although LCMO20 exhibits short-range polaron ordering (Ref. 19) it is unclear how such ordering can produce structural changes that so dramatically affect the spin excitations.
[32] The sharpness of the spin-wave excitations in Fig. 1 suggests that the broadening of $\chi_{\mathbf{q}}$ and the finite ξ in Fig. 6 are intrinsic and not due to the composition fluctuations.
[33] E. Dagotto, T. Hotta, and A. Moreo, Phys. Rep. **344**, 1 (2001).
[34] M. Fäth, S. Freisem, A. A. Menovsky, Y. Tomioka, J. Aarts, and J. A. Mydosh, Science **285**, 1540 (1999).
[35] G. Biotteau, M. Hennion, F. Moussa, J. Rodriguez-Carvajal, L. Pinsard, A. Revcolevschi, Y. M. Mukovskii, and D. Shulyatev, Phys. Rev. B **64**, 104421 (2001).